Diffusive transport of light in three-dimensional disordered Voronoi structures

Zeinab Sadjadi and MirFaez Miri*
Institute for Advanced Studies in Basic Sciences (IASBS), P. O. Box 45195-1159, Zanjan 45195, Iran

Holger Stark
Institut für Theoretische Physik, Technische Universität Berlin, Hardenbergstrasse 36, D-10623 Berlin, Germany
(Received 5 February 2008; published 12 May 2008)

The origin of diffusive transport of light in dry foams is still under debate. In this paper, we consider the random walks of photons as they are reflected or transmitted by liquid films according to the rules of ray optics. The foams are approximately modeled by three-dimensional Voronoi tessellations with varying degree of disorder. We study two cases: A constant intensity reflectance and the reflectance of thin films. Especially in the second case, we find that in the experimentally important regime for the film thicknesses, the transport-mean-free path l^* does not significantly depend on the topological and geometrical disorder of the Voronoi foams including the periodic Kelvin foam. This may indicate that the detailed structure of foams is not crucial for understanding the diffusive transport of light. Furthermore, our theoretical values for l^* fall in the same range as the experimental values observed in dry foams. One can therefore argue that liquid films contribute substantially to the diffusive transport of light in dry foams.

DOI: 10.1103/PhysRevE.77.051109 PACS number(s): 46.65.+g, 82.70.Rr, 42.25.Dd, 42.68.Ay

I. INTRODUCTION

The interaction of light with matter is a highly interesting subject with many facets. For example, multiply scattered light in turbid media is a very complex topic. However, it becomes treatable when, after a sufficiently large amount of scattering events, light reaches its diffusive limit [1]. Diffusing light is used for biomedical imaging [2] and in diffusing-wave spectroscopy (DWS) it is able to monitor dynamic processes in turbid materials [3]. Recently, even clear evidence for strong localization of light was given [4]. In colloidal suspensions and nematic liquid crystals [5] the respective scattering events and diffusion of light are well understood. But why are aqueous foams [6,7], as used, e.g, in shaving cream, turbid?

Aqueous foams consist of gas bubbles separated by liquid films [6,7]. In dry foams, where most of the liquid has drained out, the bubbles are deformed to polyhedra. The so-called Plateau rules state that always three films meet in the Plateau borders, which form a network of liquid channels throughout the foam, and that four of these borders meet at tetrahedral vertices. Foams are visibly opaque although both the gas and liquid components are transparent.

Precise light-scattering experiments show that light transport reaches its diffusive limit in foams [8–10], which means that photons perform a random walk. However, the mechanisms underlying this random walk are not well understood. One suggestion is that scattering from the Plateau borders is responsible for the diffusing light [9]. The transport-mean-free path l^*, over which the photon direction becomes randomized, is then predicted as $l^* \propto H/\sqrt{\varepsilon}$, where H is the average bubble diameter and ε is the liquid volume fraction. However, data rule this out in favor of the empirical law [9,11],

$$l^* \approx H\left(\frac{0.14}{\varepsilon} + 1.5\right). \tag{1}$$

The authors of Ref. [11] state that this may imply significant contributions from scattering from vertices [12] or films [13–17]. Transport effects, such as total internal reflection of photons inside the Plateau borders, are studied in [11,18].

In recent years we have explored how liquid films in combination with ray optics determine light transport in dry foams [13–17]. In a step-by-step approach, we employed three model foams: The honeycomb structure, two-dimensional Voronoi tessellations [19], and finally the three-dimensional Kelvin structure [7,20]. Apparently, the periodic Kelvin structure is highly idealistic. In his momentous experimental study of bubble shapes, Matzke did not find even a single Kelvin cell [21]. Therefore, in this paper, we extend our studies toward real dry foams. We introduce topological and geometrical disorder based on a three-dimensional Voronoi foam model to investigate the influence of disorder. Note that a Voronoi foam does not obey Plateau's rules, and indeed all films of a Voronoi foam are flat. Thus an accurate sample foam provided by the Surface Evolver software [22] clearly better describes the geometry of a real foam. Nevertheless, we deliberately concentrate on the Voronoi tessellations with flat films in order to greatly simplify our simulations of light transport, which are still very time consuming. Moreover, a comparison of the results presented in this paper with future theoretical studies of diffusive light transport in exact models of real foams, will highlight the role of both their geometry and their curved films.

Cells in a foam are much larger than the wavelength of light, thus one can employ ray optics and follow a light beam or photon as it is reflected by the liquid films with a probability r called the intensity reflectance. We perform extensive simulations to determine the diffusive limit of light for two models. In model I, we choose a constant intensity reflectance r to explore the effect of disorder. The essential

*miri@iasbs.ac.ir

result of our Monte Carlo simulations is summarized in the empirical formula for the transport-mean-free path l^*,

$$l^*_{\text{Voronoi}}(r) = 0.63H\frac{1-r}{r}(1-b_1+b_2r). \tag{2}$$

The main behavior of $l^*_{\text{Voronoi}}(r)$ is governed by the factor $(1-r)/r$. Quite remarkably, this factor is also found in the honeycomb, two-dimensional disordered Voronoi, and three-dimensional regular Kelvin structures. However, there is a small but systematic deviation from $(1-r)/r$, described by the last factor in Eq. (2) with $0<b_1<0.1$ and $b_2\approx 0.1$. Both constants show a slight dependence on disorder in the Voronoi foam. In model II, we use the intensity reflectance of thin films with its significant dependence on the incident angle and on d/λ, where d is film thickness and λ is the wavelength of light. Our theoretical values for the transport-mean-free path l^* fall in the same range as the experimental values for the driest foams in Ref. [9]. This shows that liquid films are important for the understanding of photon diffusion in dry foams otherwise we should have obtained much larger transport-mean-free paths. We also observe that topological and geometrical disorder do not change the qualitative behavior of l^*. Even quantitative changes are not very pronounced. Thus, our extensive numerical simulations support a conclusion that we already drew from our previous two-dimensional investigations [14]: The detailed structure of a Voronoi foam is not important for understanding the diffusive limit of light transport.

Our paper is organized as follows. In Sec. II we introduce the Voronoi tessellation as a simple model foam. Photon transport in a Voronoi structure using constant and thin-film intensity reflectances are discussed in Secs. III A and III B, respectively. Discussions, conclusions, and an outlook are presented in Sec. IV.

II. MODEL FOAM

As a simple model for a three-dimensional disordered dry foam, we choose the Voronoi tessellation [19]. Voronoi foams satisfy the topological requirements on edge and face connectivity in Plateau's rules, but not the geometric conditions; e.g., the angles between two edges are not equal to the tetrahedral angle. To make such a Voronoi foam, a distribution of seed points in the simulation box is chosen and then Voronoi polyhedrons are constructed in complete analogy to the Wigner-Seitz cells for periodic lattice sites. We start with a body-centered cubic lattice of seed points, which gives the Kelvin foam, and then systematically introduce disorder by shifting the seed points in random directions. The magnitude of the displacement vectors of the seed points is uniformly distributed in the interval $[0,h]$ and disorder in a Voronoi foam increases with h. Referring h to the diameter H_{Kelvin} of a cell in the Kelvin foam [16], we study five samples with $h/H_{\text{Kelvin}}=0.02$, 0.05, 0.07, 0.12, and 0.20. Our Voronoi foams are produced by the software Qhull [23]. Typically, the simulation box contains around 8200 cells, 62 800 films, and 11 200 edges. To simulate the diffusion of photons in these model foams, periodic boundary conditions are implemented.

In disordered foams several random variables exist; e.g., the edge length L, the cell surface S, the cell volume V, the number of faces per cell f, and the number of edges per face n. A first insight into the cellular structure can be gained through the distribution of these variables. To characterize foams and their geometrical and topological disorder, we have collected data for the following quantities:

$$\Delta L/L = \frac{[\langle L^2\rangle - \langle L\rangle^2]^{1/2}}{\langle L\rangle},$$

$$\Delta S/S = \frac{[\langle S^2\rangle - \langle S\rangle^2]^{1/2}}{\langle S\rangle},$$

$$\Delta V/V = \frac{[\langle V^2\rangle - \langle V\rangle^2]^{1/2}}{\langle V\rangle},$$

$$I_Q = \left\langle \frac{36\pi V^2}{S^3} \right\rangle,$$

$$\mu_{2,f} = \langle f^2\rangle - \langle f\rangle^2,$$

$$\mu_{2,n} = \langle n^2\rangle - \langle n\rangle^2, \tag{3}$$

where averages are denoted by $\langle\cdots\rangle$. The first three quantities give the standard deviations relative to mean values of the three respective distributions for L, S, and V. The isoperimetric quotient I_Q is one for a sphere and, therefore, measures how strongly the cells are deformed relative to a sphere. Finally, the variances $\mu_{2,f}$ and $\mu_{2,n}$ are considered as measures for topological disorder. We also note that instead of $\Delta V/V$ and I_Q, alternative measures $p=\langle V\rangle^{2/3}/\langle V^{2/3}\rangle-1$ and $\beta=\langle S/(36\pi V^2)^{1/3}\rangle$, are introduced in Ref. [24].

It is instructive to compare our samples with slightly polydisperse real foams investigated by Monnereau *et al.* [25], and random monodisperse foams simulated by Kraynik *et al.* [26], see Table I. To produce such foams, Kraynik *et al.* used the Surface Evolver software to relax an initial Voronoi structure produced from the packing of spheres. Another structure that is commonly considered the complete spatial random pattern, is the Poisson Voronoi tessellation (PVT) [19]. It allows the analytic evaluation of the moments of various distribution functions, and consequently has gained much attention. However, PVT clearly cannot serve as a model for real foams. As Table I shows, PVT possesses a high degree of topological disorder, $\mu_{2,f}=11.055$ and $\mu_{2,n}=2.49$, while in real foams $\mu_{2,f}<3.66$ and $\mu_{2,n}<0.42$ [25]. Moreover, in contrast to the simulated foams in [26], PVT has an overwhelming number of short edges, i.e., the distribution of edge lengths reaches its maximum at $L=0$ [19].

The distribution of L, S, V, f, and n for our Voronoi foams are depicted in Figs. 1–3. Note that these foams are constructed from an initial Kelvin structure, thus here L_{Kelvin}, S_{Kelvin}, and V_{Kelvin} serve as natural units of length, surface, and volume, respectively. Characteristics of the Kelvin foam, our Voronoi foams 1–5, real foams [25], simulated foams [26], and the Poisson Voronoi tessellation [19] are summarized in Table I. We shortly discuss several points. The stan-

TABLE I. Topological and geometrical characteristics of the cells in the Kelvin foam, our Voronoi foams 1–5, real foams [25], simulated foams [26], and the Poisson Voronoi tessellation (PVT) [19]. The symbols are explained in the text.

	Kelvin foam	Foam 1	Foam 2	Foam 3	Foam 4	Foam 5	Real foam	Simulation	PVT
$\Delta L/L$	0	0.050197	0.126543	0.164922	0.312005	0.486383			
$\Delta S/S$	0	0.00684	0.01768	0.02340	0.04330	0.07433			
$\Delta V/V$	0	0.011179	0.028264	0.037067	0.069619	0.122512	0.08–0.29		
I_Q	0.757	0.752663	0.748894	0.745840	0.727823	0.686616	0.694	0.693–0.751	
$\langle f \rangle$	14	14.0	14.0	14.0	14.007812	14.188232	13.5	13.7–13.94	15.535
$\langle n \rangle$	5.142857	5.142857	5.142857	5.142857	5.143335	5.154229	5.11		5.228
$\mu_{2,f}$	0	0	0	0	0.028259	0.930633	0.85–3.66	0.812–1.46	11.055
$\mu_{2,n}$	0.979593	0.979593	0.979593	0.979593	0.981509	1.028764	0.365–0.42		2.49

dard deviations and variances in Table I and the distributions in Figs. 1 and 2 clearly demonstrate that the disorder in the Voronoi foams increases with increasing displacement h of the seed points. While Voronoi foam 1 ($h/H_{\text{Kelvin}}=0.02$) with its narrow distributions is still close to the Kelvin foam, the widths of the distributions grow with increasing h and are quite broad in Voronoi foam 5 with $h/H_{\text{Kelvin}}=0.20$. This is especially visible in the distributions for edge length L, cell surface S, and cell volume V in Figs. 1 and 2. For $h/H_{\text{Kelvin}}>0.20$, the Voronoi foam approaches the Poisson Voronoi tessellation. The unit cell of a Kelvin foam consists of eight hexagonal and six square faces. This is especially visible in the bimodal distribution for the number of faces with n edges in Fig. 3, which occurs in all of our Voronoi foams 1–5. Note that foam 4 additionally contains pentagons and in foam 5 furthermore triangles and heptagons appear. In real foams, however, the distribution has its single maximum at $n=5$.

Our Voronoi foams constructed from an initial Kelvin structure, are indeed distinct from real foams, although some of the statistical characteristics of foams 4 and 5 are close to

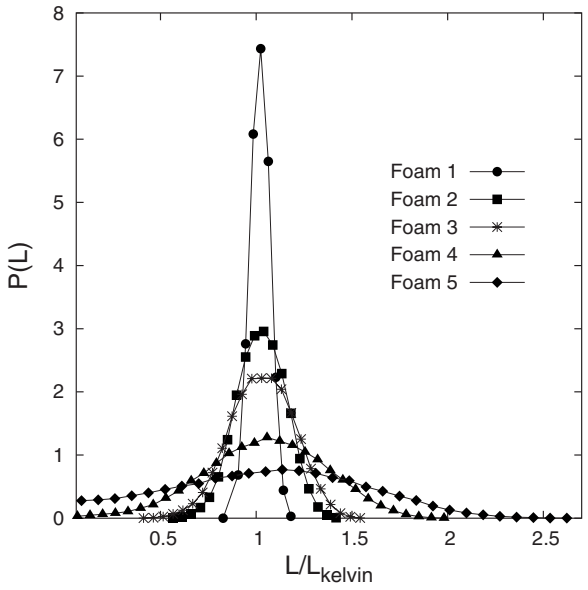

FIG. 1. Distribution of edge length (in units of L_{Kelvin}) for the disordered Voronoi foams 1–5.

or agree with the one of real foams. Nevertheless, as we have just discussed, our Voronoi foams 1–5 are characterized by increasing topological and geometrical disorder. In the following, we investigate whether this disorder does have any influence on the transport-mean-free path l^*.

III. DIFFUSIVE TRANSPORT OF LIGHT

We investigate the transport-mean-free path l^* for two models.

A. Model of constant intensity reflectance

To explore the impact of disorder on l^*, we assume here that liquid films have a constant reflectance r. We model single photon paths in a Voronoi foam as a random walk with rules motivated by ray optics, i.e., an incoming light beam is reflected from a face with a probability r or it traverses the face with a probability $t=1-r$. This naturally leads to a persistent random walk of the photons [13], where the walker remembers its direction from the previous step [27,28]. Persistent random walks are employed in biological problems [29], turbulent diffusion [30], polymers [31], Landauer diffusion coefficient for a one-dimensional solid [32], and in general transport mechanisms [33]. More recent applications are reviewed in [34].

Our computer program takes 10^4 photons at an initial position, and launches them in a direction specified by polar angles θ and φ. Then it generates the trajectory of each photon following a standard Monte Carlo procedure and evaluates the statistics of the photon cloud at times $\tau \in [10\,000, 10\,200, \ldots, 15\,800]$ (in units of $\langle L \rangle / c$, where c denotes the velocity of light). As detailed in Ref. [13], we determine the diffusion constant D from the temporal evolution of the average mean-square displacement of the photons: $\langle \mathbf{r}^2 \rangle = 6Dt$. Then the transport-mean-free path follows from

$$l^* = 3D/c. \tag{4}$$

For angles $\theta \in [3°, 20°, \ldots, 71°]$ and $\varphi \in [3°, 20°, \ldots, 156°]$, the simulation is repeated for each intensity reflectance $r \in [0.1, 0.2, \ldots, 0.9]$. As a reasonable result, no dependence on the starting point and the starting direction is observed. In Fig. 4 we plot the transport-mean-

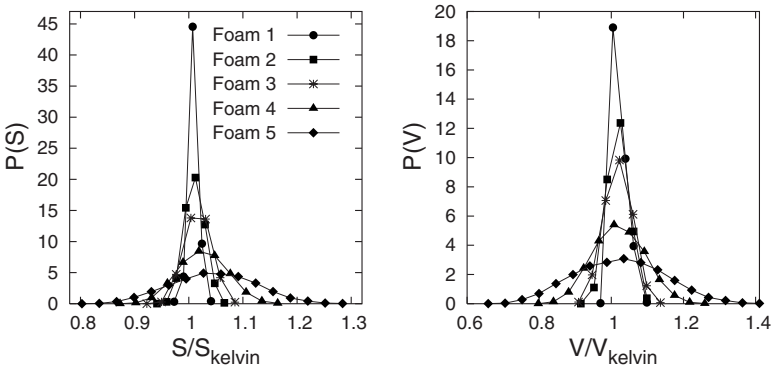

FIG. 2. Distribution of cell surface (in units of S_{Kelvin}), and distribution of cell volume (in units of V_{Kelvin}), for the disordered Voronoi foams 1–5.

free path l^* in units of the average cell diameter H as a function of r, where H is defined via $H=[6\langle V\rangle/\pi]^{1/3}$. The line is a fit to $0.63(1-r)/r$. In Fig. 4 the transport-mean-free paths l^* for the regular Kelvin foam and the disordered Voronoi foams 1–5 are not distinguishable from each other. To increase the resolution, the rescaled transport-mean-free path $l^*(r)/[0.63H(1-r)/r]$ versus r is plotted in Fig. 5. The error bars reflect the standard deviations when we average over all transport-mean-free paths $l^*(\theta,\varphi)$ for different starting positions and angles. From Fig. 5 we find that our numerical results agree well with the relation $l^*_{\mathrm{Voronoi}}(r)=0.63H\frac{1-r}{r}(1-b_1+b_2r)$ mentioned already in Eq. (1) in the introduction. Both constants b_1 and b_2 show a slight dependence on disorder in the Voronoi foam. The results here already demonstrate that disorder in the Voronoi foams does not change l^* significantly.

B. Model of thin-film intensity reflectance

In the second, more realistic model, we use the intensity reflectance of thin films. Again, we study the persistent random walk of photons to probe the influence of disorder in the Voronoi foams on the transport-mean-free path.

For a plane wave with wave vector $k\hat{\boldsymbol{k}}$ incident from the air onto a liquid film with normal vector $\hat{\boldsymbol{n}}$, the incident electric field with a general state of polarization is $\boldsymbol{E}_{\mathrm{incident}}=E_1e^{i\phi_1}\hat{\boldsymbol{e}}_1+E_2e^{i\phi_2}\hat{\boldsymbol{e}}_2+E_3e^{i\phi_3}\hat{\boldsymbol{e}}_3$, where E_m and ϕ_m are, respectively, the magnitude and phase of the field component along the unit vector $\hat{\boldsymbol{e}}_m$ $(m=1,2,3)$. Taking into account all possible multiple refraction paths in the film [35], the electric field vectors of the transmitted and reflected waves become

$$\boldsymbol{E}_{\mathrm{transmitted}}=(t_s-t_p)(\boldsymbol{E}_{\mathrm{incident}}\cdot\hat{\boldsymbol{b}})\hat{\boldsymbol{b}}+t_p\boldsymbol{E}_{\mathrm{incident}},$$

$$\boldsymbol{E}_{\mathrm{reflected}}=(r_s+r_p)(\boldsymbol{E}_{\mathrm{incident}}\cdot\hat{\boldsymbol{b}})\hat{\boldsymbol{b}}-r_p\boldsymbol{E}_{\mathrm{incident}}+2r_p(\boldsymbol{E}_{\mathrm{incident}}\cdot\hat{\boldsymbol{n}})\hat{\boldsymbol{n}},\tag{5}$$

from which one calculates the intensity reflectance $r(i)=|\boldsymbol{E}_{\mathrm{reflected}}|^2/|\boldsymbol{E}_{\mathrm{incident}}|^2$ as a function of the incident angle i of the plane wave

$$r(i)=|r_p|^2+\frac{|\boldsymbol{E}_{\mathrm{incident}}\cdot\hat{\boldsymbol{b}}|^2}{|\boldsymbol{E}_{\mathrm{incident}}|^2}(|r_s|^2-|r_p|^2).\tag{6}$$

Here $|\cdots|$ denotes the magnitude of a complex number, and $\hat{\boldsymbol{b}}=\hat{\boldsymbol{n}}\times\hat{\boldsymbol{k}}$. Details of our approach with the explicit formulas for the coefficients r_p, t_p, r_s, and t_s are given in Ref. [16]. We implemented the reflectance $r(i)$ of Eq. (6) in our Monte Carlo simulations. Again, we used the launching directions for the photons as mentioned in Sec. III A, but evaluated the statistics of the photon cloud at times $\tau\in[30\,000,30\,200,\ldots,35\,800]$ (in units of $\langle L\rangle/c$). Note that the thin-film reflectance is small except near the grazing incidence, thus long simulation times are required to achieve the accuracy reported in Sec. III A.

The reflectance r crucially depends on the ratio d/λ of film thickness d and wavelength λ of light, the refractive index n_0 of the film, and the incident angle i. Note that even in films as thin as the common black film, r increases to 1 close to grazing incidence $(i\to 90°)$. This feature basically explains why films significantly contribute to the diffusion of light in aqueous foams [14,16].

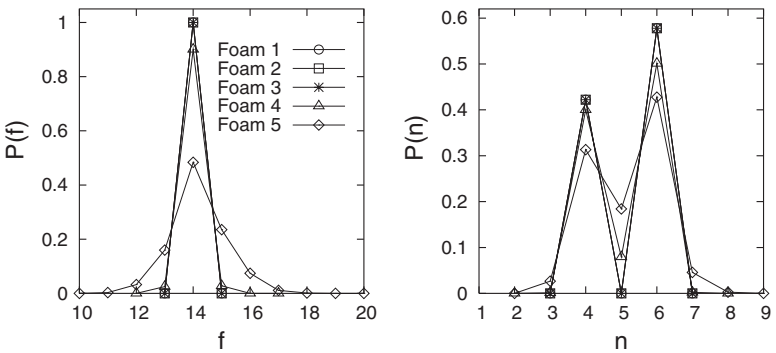

FIG. 3. Distribution of cells with f faces, and distribution of faces with n edges, for the disordered Voronoi foams 1–5.

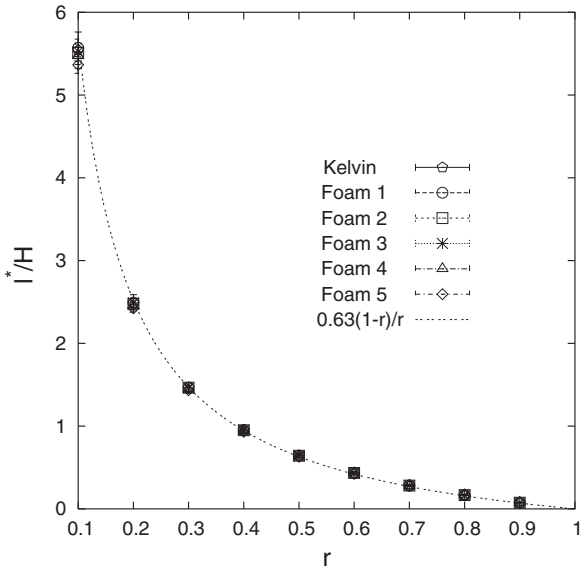

FIG. 4. The transport-mean-free path l^* (in units of the average cell diameter H) as a function of intensity reflectance r, for the Kelvin and the disordered Voronoi foams 1–5. The Monte Carlo simulation results and the fit $l^*(r)/H=0.63(1-r)/r$ are denoted, respectively, by points and line.

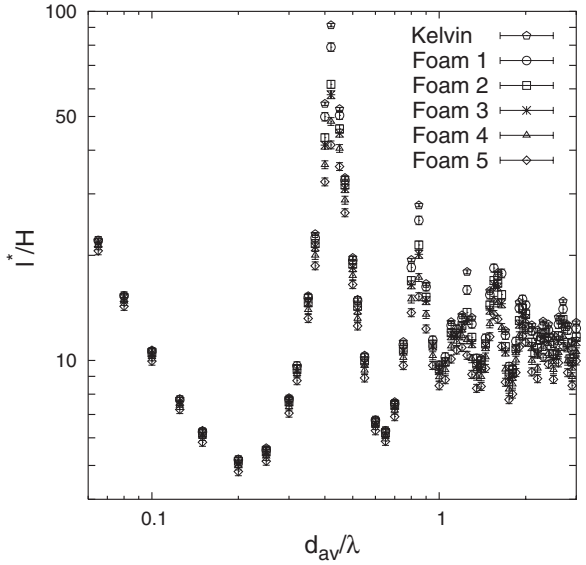

FIG. 6. The transport-mean-free path l^* (in units of the average cell diameter H) as a function of d_{av}/λ for the Kelvin foam and disordered Voronoi foams 1–5. The refractive index n_0 of the liquid phase is 1.34.

First, we assume that all films of the foam have the same thickness d_{av}. In Fig. 6 we plot l^* as a function of d_{av}/λ for the Kelvin foam and our disordered Voronoi foams 1–5. For $d_{av}/\lambda<0.2$, the transport-mean-free path monotonically decreases as d_{av} increases. There is a pronounced minimum around $d_{av}/\lambda=0.2$. Between $d_{av}/\lambda=0.2$ and 3 oscillations exist that are due to oscillations in the reflectance r of a thin film. The oscillations are reduced for more disordered foams but do not disappear. The transport-mean-free path l^* exhibits two strong maxima around $d_{av}/\lambda=0.43$ and 0.84. A closer inspection of Fig. 6 shows that the heights of the pronounced maxima at $d_{av}/\lambda=0.43$ and 0.84 decrease as the disorder increases. To explain this behavior, we note that in the Kelvin structure, long straight photon paths can cross parallel faces. These long photon paths occur for the parallel polarization state since below the Brewster angle the reflectance is small and especially for the most pronounced maximum at $d_{av}/\lambda=0.43$ close to zero [16]. With increasing disorder in the Voronoi foams these parallel faces and, therefore, long straight photon paths, disappear. In Fig. 6 the transport-mean-free paths l^* for the regular Kelvin foam and the disordered Voronoi foams 1–5 are not distinguishable from each other in the region of $d_{av}/\lambda<0.3$. To increase the resolution, the rescaled transport-mean-free path l^*/l^*_{Kelvin} of Voronoi foams 1–5 is plotted for this region in Fig. 7. Clearly, the transport-mean-free paths differ from each other by at most 10%.

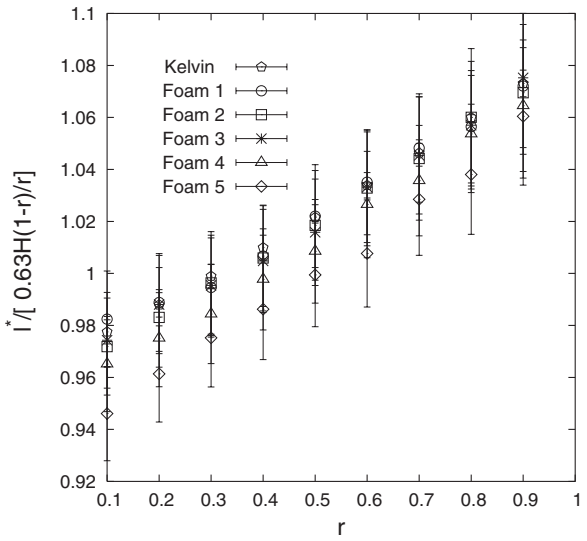

FIG. 5. The transport-mean-free path l^* plotted relative to $0.63H(1-r)/r$ as a function of intensity reflectance r. We find that $l^*_{\text{Voronoi}}(r)=0.63H(1-r)/r(1-b_1+b_2r)$ with $0<b_1<0.1$ and $b_2\approx 0.1$.

Second, in our model we introduce some additional randomness in the thickness d of the films assuming that it is uniformly distributed in $[d_{av}-d_w,d_{av}+d_w]$, where d_{av} denotes the average thickness and d_w the width of the distribution. In Fig. 8 we plot l^* as a function of d_{av}/λ for Voronoi foam 4 with various thickness distributions. Other disordered Voronoi foams show the same behavior. Obviously, disorder in d decreases the oscillations to an approximately constant transport-mean-free path for $d_{av}/\lambda>1$. The two strong maxima are reduced noticeably and ultimately disappear for strong disorder in the film thickness, as illustrated by the data for $d_w/d_{av}=0.5$ and 0.9. However, we still observe that moderate disorder in the thickness ($d_w/d_{av}\leq 0.2$) does not affect l^* and its monotonic behavior for $d_{av}/\lambda<0.2$.

IV. DISCUSSION, CONCLUSIONS, AND OUTLOOK

To understand the role of liquid films for light transport in dry foams, we started with the two-dimensional honeycomb

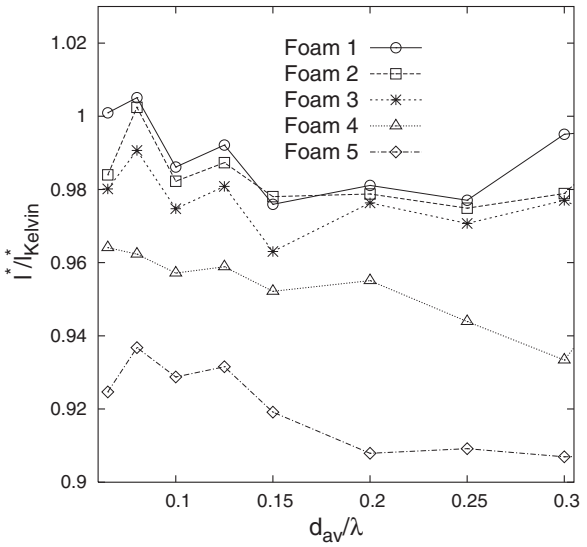

FIG. 7. The transport-mean-free path l^* of Voronoi foams 1–5 plotted relative to l^*_{Kelvin} as a function of d_{av}/λ. For all these foams, $d_w=0$.

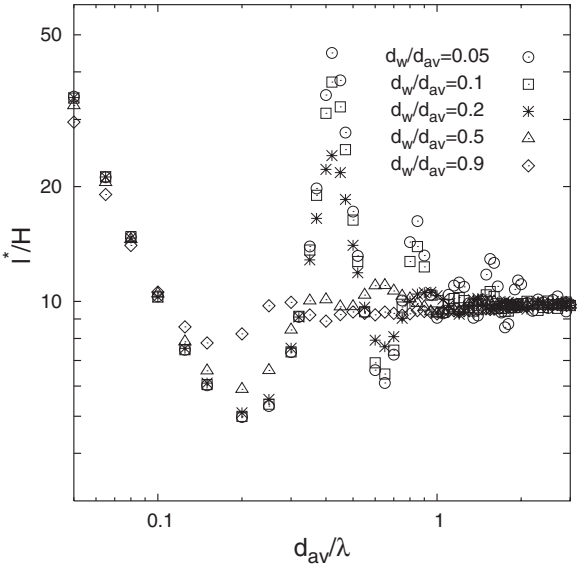

FIG. 8. The transport-mean-free path l^* (in units of the average cell diameter H) as a function of d_{av}/λ for Voronoi foam 4 with various thickness distribution. Note, for $d_w/d_{av}=0.5$ and 0.9, the pronounced maximum disappears.

[13] and Voronoi structures [14]. Then we focused on the Kelvin foam [16] to explore the effect of space dimension. The Kelvin foam is periodic in space, while real foams are disordered. To investigate the influence of topological and geometrical disorder on diffusive photon transport, we have utilized in this paper the three-dimensional Voronoi tessellations.

We have studied the photon's persistent random walk in a three-dimensional Voronoi structure based on rules motivated by ray optics. In a first model, we used a constant intensity reflectance r. The interesting result is that the transport-mean-free path for the honeycomb structure, the two-dimensional Voronoi foam, the three-dimensional Kelvin structure, and the three-dimensional Voronoi foam are all determined by the same factor $(1-r)/r$ for constant intensity reflectance r in spite of the differences in dimension and structure. For the two-dimensional Voronoi foams, we even see the same behavior as in Eq. (1) but with the prefactor 0.63 replaced by 0.55. Finally, the results here already demonstrate that disorder in the Voronoi foams does not change l^* significantly (see Figs. 4 and 5). This confirms our speculation in Refs. [13–16] that neither the dimension of space nor disorder have a strong influence on the magnitude of the transport-mean-free path. Note that the factor $(1-r)/r$ expresses the fact that independent of the dimension of space and the different shapes of the cells in a foam, photon transport is ballistic for $r=0$, and that photons stay confined to the initial cell for $r=1$.

In a second, more realistic model, we used the intensity reflectance of a thin film, with its significant dependence on film thickness d_{av} and angle of incidence i. Close to grazing incidence ($i\rightarrow 90°$), the reflectance always sharply increases to 1. Thus, a thin film, even as thin as the common black film, randomizes the photon direction and contributes to l^*. Based on extensive Monte Carlo simulations, we paid special attention to the behavior of l^* at small d_{av}/λ: In real foams $d_{av}<100$ nm [36] and, combined with the visible portion of the spectrum (450 nm$<\lambda<$750 nm), one arrives at $d_{av}/\lambda<0.2$ as the relevant region in explaining the measurements of the transport-mean-free path in Ref. [9]. Quite interesting, we found that the monotonic behavior of l^* for $d_{av}/\lambda<0.2$ does not show a significant dependence on the detailed geometrical structure of our Voronoi foams and on moderate disorder in the film thickness (see Figs. 6–8).

Real foams obey Plateau's laws. They state the following: (i) Each film has a constant mean curvature; (ii) three films meet at angles of 120° at each Pleateau border; and (iii) these borders meet in fours at the tetrahedral angle $[\arccos(-1/3)=109.47°]$ to form a vertex. A Kelvin foam with flat faces of its cells approximately obeys the second and third law; however, a disordered Voronoi foam does not. We found that the transport-mean-free path of the Kelvin and the Voronoi structures deviate from each other by at most 10% in the experimentally relevant region for d_{av}/λ. This is an indication that fulfilling Plateau's second and third laws is of minor importance when one tries to understand the role of liquid films for diffusive transport of light in foams. Even the slight curvature of the films might not be very important since in the ray optics approach it just introduces some additional randomness in the relevant surface normal which varies across the film. Future investigations on realistic foam structures, e.g., constructed by the Surface Evolver software will clarify all of these aspects.

Vera, Saint-Jalmes, and Durian observed the empirical law stated in Eq. (1) for $0.008<\varepsilon<0.3$. Experimental values for l^*/H increase from 2 to 20 for decreasing ε, whereas we determine a range of l^*/H between 5 (for $d_{av}/\lambda=0.2$) and 25 (for $d_{av}/\lambda=0.06$, i.e., for a common black film) as illustrated in Fig. 6. That means our theoretical values for l^* fall in the same range as the experimental values for the driest foams in Ref. [9]. This shows that liquid films are important for the understanding of photon diffusion in dry foams, otherwise

we should have obtained much larger transport-mean-free paths. However, to compare our theoretical findings to experiments, we should know the contribution of the Plateau borders to l^*. After all, even in a rather dry foam with a liquid fraction of 1%, most of the liquid resides in these borders and their junctions. Furthermore, a relation between the film thickness d_{av} and the liquid volume fraction ε is needed. To the best of our knowledge, systematic measurements of the film thickness in dry foams have not been reported, neither do theoretical models exist. In the case of dense oil-in-water emulsions, the dependence of the film thickness on the oil-volume fraction has been modeled by Buzza and Cates [37]. However, their results cannot be applied directly to foams.

In this paper, we focused on the contribution of liquid films to the transport-mean-free path of photon diffusion in dry foams. To achieve a complete understanding of the subject, there is still much to do. Of immediate interest are modeling of the film thickness variation with the liquid volume fraction and following the random walk of photons by taking into account both their refraction at thin films and their scattering from Plateau borders. To the best of our knowledge, the scattering matrix for a Plateau border is not available. However, ray optics reveal intriguing optical properties of the Plateau borders [38,39]. Using the hybrid lattice gas model for two-dimensional foams, Sun and Hutzler [38] emphasize that the complex geometry of the Plateau borders affects the optical properties of foams. However, Plateau borders of a two-dimensional foam do not form a network and channeling of the photons, as observed in Ref. [11], is impossible. Thus an extension of Ref. [38] to three-dimensional foams would be interesting.

ACKNOWLEDGMENTS

MF.M. and Z.S. thank Iran's Ministry of Science, Research and Technology for support of the parallel computing facilities at IASBS under Grant No. 1026B(503495), Iranian Telecommunication Research Center (ITRC) for financial support, and Farhad Abdi for technical assistance. H.S. appreciates discussions with Regine von Klitzing.

[1] P. Sheng, *Introduction to Wave Scattering, Localization, and Mesoscopic Phenomena* (Academic, San Diego, 1995).
[2] A. Yodh and B. Chance, Phys. Today **48**(3), 34 (1995).
[3] G. Maret and P. E. Wolf, Z. Phys. B: Condens. Matter **65**, 409 (1987); D. J. Pine, D. A. Weitz, P. M. Chaikin, and E. Herbolzheimer, Phys. Rev. Lett. **60**, 1134 (1988).
[4] C. M. Aegerter, M. Störzer, and G. Maret, Europhys. Lett. **75**, 562 (2006).
[5] B. A. van Tiggelen, R. Maynard, and A. Heiderich, Phys. Rev. Lett. **77**, 639 (1996); H. Stark and T. C. Lubensky, *ibid.* **77**, 2229 (1996); B. A. van Tiggelen and H. Stark, Rev. Mod. Phys. **72**, 1017 (2000).
[6] D. Weaire and N. Rivier, Contemp. Phys. **25**, 59 (1984).
[7] D. Weaire and S. Hutzler, *The Physics of Foams* (Oxford University Press, New York, 1999).
[8] D. J. Durian, D. A. Weitz, and D. J. Pine, Science **252**, 686 (1991); Phys. Rev. A **44**, R7902 (1991).
[9] M. U. Vera, A. Saint-Jalmes, and D. J. Durian, Appl. Opt. **40**, 4210 (2001).
[10] J. C. Earnshaw and A. H. Jaafar, Phys. Rev. E **49**, 5408 (1994); A. D. Gopal and D. J. Durian, J. Colloid Interface Sci. **213**, 169 (1999); A. D. Gopal and D. J. Durian, Phys. Rev. Lett. **91**, 188303 (2003); R. Höhler, S. Cohen-Addad, and H. Hoballah, *ibid.* **79**, 1154 (1997); S. Cohen-Addad and R. Höhler, *ibid.* **86**, 4700 (2001); S. Cohen-Addad, R. Höhler, and Y. Khidas, *ibid.* **93**, 028302 (2004).
[11] A. S. Gittings, R. Bandyopadhyay, and D. J. Durian, Europhys. Lett. **65**, 414 (2004).
[12] S. Skipetrov (unpublished).
[13] M. F. Miri and H. Stark, Phys. Rev. E **68**, 031102 (2003).
[14] M. F. Miri and H. Stark, Europhys. Lett. **65**, 567 (2004).
[15] M. F. Miri and H. Stark, J. Phys. A **38**, 3743 (2005).
[16] M. F. Miri, E. Madadi, and H. Stark, Phys. Rev. E **72**, 031111 (2005).
[17] M. F. Miri, Z. Sadjadi, and M. E. Fouladvand, Phys. Rev. E **73**, 031115 (2006).
[18] M. Schmiedeberg, M. F. Miri, and H. Stark, Eur. Phys. J. E **18**, 123 (2005).
[19] A. Okabe, B. Boots, and K. Sugihara, *Spatial Tessellations, Concepts and Applications of Voronoi Diagrams* (Wiley, Chichester, 2000).
[20] *The Kelvin Problem*, edited by D. Weaire (Taylor and Francis, London, 1996).
[21] E. B. Matzke, Am. J. Bot. **33**, 58 (1946).
[22] K. Brakke, Exp. Math. **1**, 141 (1992); http://www.susqu.edu/facstaff/b/brakke/evolver/
[23] http://www.qhull.org
[24] A. M. Kraynik, D. A. Reinelt, and F. van Swol, Phys. Rev. Lett. **93**, 208301 (2004).
[25] C. Monnereau, B. Prunet-Foch, and M. Vignes-Adler, Phys. Rev. E **63**, 061402 (2001).
[26] A. M. Kraynik, D. A. Reinelt, and F. van Swol, Phys. Rev. E **67**, 031403 (2003).
[27] J. W. Haus and K. W. Kehr, Phys. Rep. **150**, 263 (1987).
[28] G. H. Weiss, *Aspects and Applications of the Random Walk* (North-Holland, Amsterdam, 1994).
[29] R. Fürth, Ann. Phys. **53**, 177 (1917).
[30] G. I. Taylor, Proc. London Math. Soc. **s2–20**, 196 (1922).
[31] P. J. Flory, *Statistical Mechanics of Chain Molecules* (Interscience, New York, 1969).
[32] S. Godoy, Phys. Rev. E **56**, 4884 (1997); S. Godoy, L. S. García-Colín, and V. Micenmacher, *ibid.* **59**, 6180 (1999).
[33] H. Larralde, Phys. Rev. E **56**, 5004 (1997); M. Boguñá, J. M. Porrà, and J. Masoliver, *ibid.* **58**, 6992 (1998); M. Boguñá, J. M. Porrà, and J. Masoliver, *ibid.* **59**, 6517 (1999); J. Dunkel, P. Talkner, and P. Hänggi, Phys. Rev. D **75**, 043001 (2007).
[34] G. H. Weiss, Physica A **311**, 381 (2002).
[35] J. R. Reitz, F. J. Milford, and R. W. Christy, *Foundations of*

Electromagnetic Theory (Addison-Wesley, Reading, 1979).
[36] M. U. Vera and D. J. Durian, Phys. Rev. Lett. **88**, 088304 (2002); S. A. Koehler, S. Hilgenfeldt, and. H. A. Stone, Langmuir **16**, 6327 (2000).
[37] D. M. A. Buzza and M. E. Cates, Langmuir **9**, 2264 (1993).
[38] Q. Sun and S. Hutzler, Colloids Surf., A **309**, 182 (2007).
[39] A. van der Net, L. Blondel, A. Saugey, and W. Drenckhan, Colloids Surf., A **309**, 159 (2007).